Fluorescence Spectroscopy Studies of Crossed Aldol Reactions: A Reactive Nile Red Dye Reveals Catalyst-Dependent Product Formation

SCHOLARONE™
Manuscripts

Fluorescence Spectroscopy Studies of Crossed Aldol Reactions: A Reactive Nile Red Dye Reveals Catalyst-Dependent Product Formation

Judith Bautista-Gomez,[†] Abdulhafiz Usman,[‡] Man Zhang,[†] Ryan J. Rafferty,[†] Stefan H. Bossmann,[†] Keith L. Hohn,*,[‡] and Daniel A. Higgins*,[†]

[†]Department of Chemistry and [‡]Department of Chemical Engineering, Kansas State University, Manhattan, Kansas 66506, United States

ABSTRACT

The synthesis of a new Nile Red derivative incorporating a reactive aldehyde moiety (NR-CHO) is reported and its use in spectroscopic studies of heterogeneous catalyst activity in crossed aldol reactions is demonstrated. ^{1}H and ^{13}C NMR, and high-resolution mass spectrometry confirmed the desired NR-CHO was obtained. Mg-Zr-Cs doped silica ($Cs(Zr,Mg)-SiO_2$) was employed as the catalyst and its performance was compared to that of commercially available MgO. Fumed silica was used as a control. Aldol reactions with acetone and acetophenone were run in 4:1 (v/v) DMSO:ketone solutions in the presence of both dilute (1 μM) and concentrated (1 mM) NR-CHO. NR-CHO fluorescence spectra were acquired as the reactions progressed. Shifts in its emission spectrum are used to distinguish the products formed and to characterize the reaction rate. The dye exhibits different behavior that defines whether the reaction stops at the addition (alcohol) product, or forms both addition and condensation (olefin) products, providing valuable initial information on catalyst activity. The assignment of addition and condensation products is supported by thin layer chromatography, high performance liquid chromatography (HPLC), and HPLC-mass spectrometry data. Product formation is shown to depend upon the catalyst employed, with the $Cs(Zr,Mg)-SiO_2$ yielding both addition and condensation products, while MgO yields primarily addition products. The advantages of NR-CHO in spectroscopic studies of aldol reactions are also demonstrated relative to commercially available 3-perylene-carboxaldehyde. The NR-CHO reported here and the results obtained will facilitate a broad range of both ensemble

2

and single molecule spectroscopic investigations of heterogeneous catalysis in crossed aldol reactions in the future.

KEYWORDS

Crossed aldol reactions, heterogeneous catalysis, in-situ investigations, fluorescence detection.

INTRODUCTION

Aldol reactions represent common and widely used synthetic routes to carbon-carbon bond formation via the coupling of, for example, an aldehyde and a ketone. The synthesis of pharmaceuticals, industrial feedstocks, commodity chemicals, and biomass-derived renewable liquid fuels frequently involve aldol reactions. These reactions are most often catalyzed by homogeneous catalysts comprising solutions of strong base (i.e., hydroxide)[1] or transition-metals.[2] However, homogeneous catalysts can be difficult to recover and reuse, producing excess waste and leading to increased cost. Heterogeneous catalysts are now being widely explored as a means to overcome these difficulties.[3-5]

Silica-based materials form an important class of porous solids now being investigated for use in heterogeneous catalysis of aldol reactions.[6-8] Catalytic sites are readily incorporated into porous silica by addition of appropriate transition metals[9-10] or acidic and basic moieties[11-13] during materials synthesis. For example, alkali or alkaline earth metals may be incorporated into the silica to form Brønsted base sites,[9-10, 14] while the silanol groups intrinsic to the silica act as Brønsted acid sites.[15-16] Bifunctional materials that incorporate both acid and base sites have been found to be particularly effective in catalyzing aldol condensation reactions.[9-10, 17] The base sites appear to best catalyze the initial aldol addition step, forming an alcohol product, while a combination of base and weak acid sites in close proximity to each other catalyze the subsequent dehydration to obtain the final olefin product.[15, 18]

It is generally accepted that both the concentration and strength of acid and base sites define the catalyst activity.[19] These parameters are most commonly determined *ex situ* by methods such as temperature programmed desorption of ammonia and carbon dioxide.[20-23] The results of such studies afford little direct information on the *in situ* acidity and basicity of the catalytic sites, which

are certain to vary with the solvent employed and the temperature at which the reaction is run, among other factors. Furthermore, the properties of the individual catalyst particles are expected to be intrinsically variable. To overcome some of the limitations of *ex situ* studies, fluorogenic reactions have been employed previously as a means to characterize catalyst activity *in situ* for a number of processes.[24-26] Many such studies have been performed by ensemble spectroscopic methods, but when highly fluorescent reactants and products are involved, the reactions can even be followed at the single molecule/single turnover level.[27-33] While fluorescence has been used previously to follow aldol reactions,[34-35] no such studies have been reported at the single molecule level to date. The dearth of single molecule studies likely stems from the lack of suitable dyes designed to undergo aldol reactions while also remaining sufficiently fluorescent for detection at the single molecule level.

In this paper, we report the synthesis of a new derivative of Nile Red that incorporates a reactive aldehyde moiety (NR-CHO). NMR spectroscopy and high-resolution mass spectrometry were used to confirm that NR-CHO was obtained, and its use in solution-phase ensemble spectroscopic studies of the heterogeneous catalysis of crossed aldol reactions was demonstrated. The Nile Red chromophore was selected for use because it is now widely employed in single molecule detection, spectroscopy, and tracking studies.[36-39] Because its lowest energy electronic transition involves an intramolecular charge transfer process,[40] its spectrum is highly dependent on its surroundings.[41] Thus, we hypothesize that subtle changes to its structure occurring during an aldol reaction will also lead to detectable changes in its fluorescence spectrum. We compare its performance to that of a commercially available 3-perylenecarboxaldehyde. We employ Mg-Zr-Cs doped silica (Cs(Zr,Mg)-SiO$_2$)[42] as the heterogeneous catalyst and compare its performance to that of commercially available MgO. The activities of these two catalysts are compared to that

of fumed silica. The occurrence of an aldol reaction and the assignment of the products formed are supported by thin layer chromatography, high performance liquid chromatography (HPLC), and HPLC-mass spectrometry (HPLC-MS) data. Changes in dye fluorescence observed during the reaction are recorded and used as a simple, real-time, *in situ* method for following reaction progress. The new NR-CHO dye reported and the results obtained in ensemble studies of aldol reactions will be useful to others seeking *in situ* methods to characterize the activity of heterogeneous catalysts. They will also facilitate future studies of catalyst activity at the single particle and single reaction event level via the implementation of single molecule spectroscopic methods. Such studies are now underway in our labs.

EXPERIMENTAL SECTION

Materials

Except as indicated below, all solvents, starting materials, and reagents employed in the synthesis of NR-CHO and Cs(Zr,Mg)-SiO$_2$ were obtained from commercial sources and used as received.

Methods for Heterogeneous Catalysts

Preparation of Cs(Zr,Mg)-SiO$_2$ catalyst. Fumed silica (Sigma-Aldrich, 99.8%) was calcined in flowing air at 500 °C for 3 h in a furnace (Barnstead F1500). The silica was then impregnated with aqueous solutions of Mg(NO$_3$)$_2$ · 6H$_2$O, ZrO(NO$_3$)$_2$ · xH$_2$O and CsNO$_3$ (Sigma-Aldrich) to yield particles incorporating theoretical loadings of magnesium, zirconium, and cesium at 0.025 wt.%, 0.033 wt.% and 13 wt.%, respectively. The aqueous mixture was subsequently immersed and sonicated at 40 °C for 24 h, followed by drying in an oven overnight at 90 °C. The catalyst was calcined in flowing air at 500 °C for 3 h prior to use.

Catalyst structural characterization. X-Ray diffraction (XRD) patterns of the as-synthesized Cs(Zr,Mg)-SiO$_2$, the commercially available MgO (Nanoscale Materials), and fumed silica were obtained using a desktop X-ray diffractometer (Rigaku Miniflex II). Transmission electron microscopy (TEM) images were acquired using a FEI Tecnai G2 Spirit BioTWIN microscope operating at 120 kV. Samples were prepared by dispersing them in ethanol, sonicating them, and then depositing them on a microgrid before imaging. Scanning electron microscopy (SEM) images were obtained using a Hitachi S-3500N microscope operating at 20 kV. The catalyst samples were sputter coated with palladium before imaging.

BET surface area and pore size distribution measurements were made on a Micromeritics ASAP 2020 Surface Area and Porosity Analyzer. Samples were first dehydrated in a 1430 series VWR vacuum oven for 24 h at 150 °C and < 77 Torr. To avoid undesirable interactions with atmospheric moisture, samples were kept in a humidity-free environment in a Sanplatec Dry Keeper Auto Desiccator Cabinet. Prior to surface area and porosity measurements, all samples went through an outgassing step for 12 h at 350 °C under vacuum. Nitrogen sorption isotherms were collected at 77 K over a relative pressure range of 0.05 to 0.995 (p/p$_0$), measured every 120 min. Mesopore-size distribution was evaluated by the nitrogen desorption isotherm and by the BJH method.[43] Total surface area was calculated by the BET method.[44] Total pore volume was determined by the amount of nitrogen adsorbed at a relative pressure of 0.99 (p/p$_0$).

Catalyst chemical characterization. Elemental analysis was accomplished by energy-dispersive X-ray spectroscopy (EDS) employing an Oxford detector (< 135 eV). The elemental composition of the catalysts was also determined using a Varian 720-ES inductively coupled plasma-optical emission spectrometer (ICP-OES). Samples were digested in nitric acid for this analysis. X-ray photoelectron spectroscopy (XPS) data were acquired using a Thermo Scientific

K-alpha[+] XPS with a monochromatic Al Kα X-ray source (1486.6 eV). XPS spectra were acquired using a 400 μm spot size, 50.0 eV pass energy, and 0.100 eV step size. The binding energies were corrected for charge shifts using the C (1s) peak of adventitious carbon at 284.8 eV as a reference.[18] Deconvolution of the XPS data was done using OriginPro software.

The acid-base properties of the catalysts were determined by temperature-programmed desorption (TPD) of CO_2 and NH_3 (Altamira Instruments AMI-200). For CO_2 TPD, 150 mg of catalyst was placed in a quartz tube and treated in helium flow at 450 °C for 1 h, with a heating rate of 10 °C/min. After cooling to 50 °C, a 10% CO_2-He mixture was passed over the samples for 30 min followed by a purge with pure helium until the baseline became stable. Desorption of CO_2 was accomplished by exposing the sample to a helium flow while heating to 500 °C at a rate of 10 °C/min. The same process was employed for NH_3 TPD using a 1% NH_3-He mixture. The desorption profile for both gases was recorded using a thermal conductivity detector.

Methods for Aldol Reactions

General procedure for crossed aldol reactions. The experimental conditions for aldol reactions were obtained from Sakthivel et al.[45] A stock solution of NR-CHO (7 mM) was prepared in DMSO (Fisher) and later used in the preparation of diluted solutions for aldol reactions. All experiments employed either ACS grade acetone (Fisher) or GC grade acetophenone (Sigma-Aldrich, > 99%) as the ketone. The ketones were each dissolved in DMSO in a 1:4 (v/v) ratio. Fluorescence measurements of the reaction kinetics employed low (1 μM) NR-CHO concentrations, while HPLC and HPLC-MS analyses were performed for reactions using high (1 mM) NR-CHO concentrations. The performance of the $Cs(Zr,Mg)$-SiO_2 catalyst was compared to that of commercially available MgO, and fumed silica. The latter served as a control. Aldol reactions and controls employed a catalyst loading of 3.07 mg/mL and reaction volumes of either

3.250 mL or 1.625 mL. The reactions were stirred at room temperature for various times, as specified below. Aldol reactions are known to depend on temperature, but such effects were excluded from the present investigations. Therefore, heat transfer from the magnetic stir plate into the reaction mixture was prevented by placing an insulating material between the stir plate and the reaction cell.

Crude products from the aldol reactions employing 1 mM NR-CHO were prepared for HPLC-MS characterization by adding one volume equivalent of saturated aqueous NH_4Cl to the mixture and then extracting 2-3 times with ethyl acetate (Fisher). The combined organic fractions were dried over anhydrous sodium sulfate (Fisher) and concentrated under vacuum. The products were dissolved in 3:2 (v/v) HPLC grade acetonitrile (Fisher) and HPLC grade water (Fisher) and analyzed using an Acquity Ultra Performance HPLC-MS (Waters). The HPLC employed a water-acetonitrile mobile phase gradient and a C18 reversed phase silica column (Cortecs). Products eluting from the column were detected by their UV absorbance at 230-300 nm. MS detection employed an electrospray ionization source. An Ultimate 3000 HPLC (Thermo Fisher) with absorbance detection at 575 nm was employed for quantitative analysis of the aldol products. A water-acetonitrile mobile phase gradient and a C18 reversed phase silica column (Thermo Fisher) were also employed here.

Fluorescence studies of crossed aldol reactions. Fluorescence spectra were acquired on a FluoroMax-2 spectrophotometer (Jobin Yvon Spex) using a Xenon lamp (150 W) as the light source. Aldol reactions were run in a quartz fluorimeter cell (Starna Cells) with a 10 mm pathlength. The cell was sealed with a Teflon cap and parafilm to prevent solvent evaporation during the reaction. Excitation and emission spectra were acquired primarily from 1 μM NR-CHO solutions. While spectra were also acquired from 1 mM NR-CHO solutions, these were severely

distorted by inner filter effects and were not used in any spectroscopic analyses. The emission spectrum of NR-CHO was recorded from 578 to 800 nm, while exciting at 575 nm. The progress of the aldol reactions was monitored in real time by recording fluorescence spectra at various time intervals during the reaction.

As described in Supplementary Information, the utility of the newly synthesized NR-CHO dye in studies of crossed aldol reactions was compared to that of a commercially available 3-perylenecarboxaldehyde dye (TCI, > 95%). In this case, 1 μM 3-perylenecarboxaldehyde solutions were employed. The 3-perylenecarboxaldehyde emission spectrum was recorded from 470 to 800 nm, while exciting at 465 nm.

Synthesis of NR-CHO

Synthesis of the aldol-reactive derivative of Nile Red, 9-diethylamino-5*H*-benzo[α]phenoxazine-5-one-2-carboxaldehyde (NR-CHO), required six steps and is based upon a previously reported synthesis of Nile Red.[46] The steps employed are shown in Scheme 1. Analytical thin layer chromatography (TLC) was employed to track reaction progress using silica gel 60 F_{254} (Merck) TLC plates. Column chromatography was employed for product purification and employed silica gel 60 (230-400 mesh) as the stationary phase. ^{1}H and ^{13}C NMR spectra were acquired on either 600 MHz (Bruker Avance III HD) or 400 MHz (Bruker Avance NEO) spectrometers. Fourier transform infrared (FTIR) spectra were taken using disposable polyethylene IR cards (Aldrich) as the sample support. Spectra were recorded in transmission mode on a Cary 630 FTIR (Agilent). High-resolution mass spectra were acquired on a LCT Premier Mass Spectrometer (Waters), using electron impact ionization.
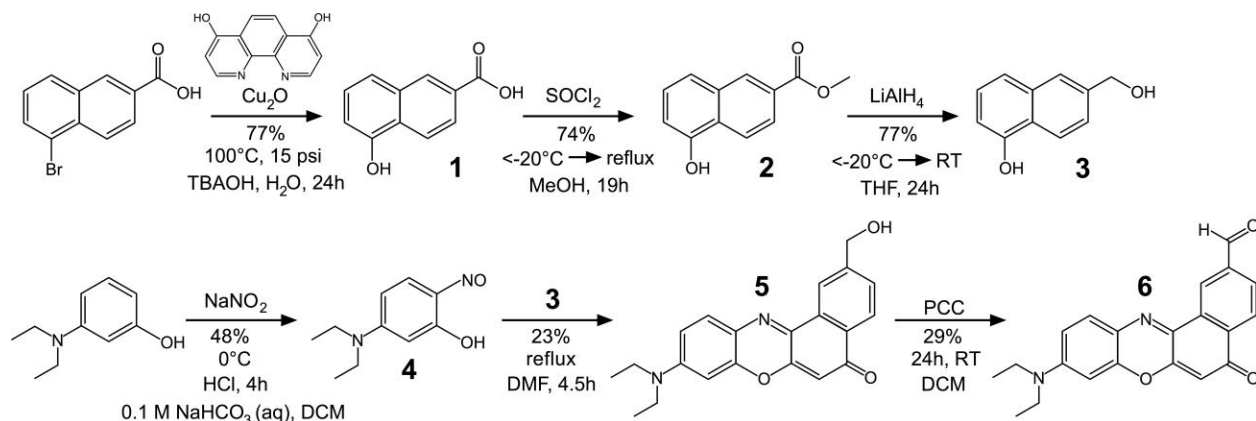
Scheme 1. Synthesis of 9-diethylamino-5*H*-benzo[α]phenoxazin-5-one-2-carboxaldehyde (NR-CHO), **6**. Product yields are given below each reaction arrow.

Synthesis of 5-hydroxy-2-naphthoic acid (**1**). The synthetic procedure reported by Wang et al. was modified to prepare **1**.[47] A 50 mL reactor (Parr 5500 series) equipped with a mechanical mixer was charged with 5-bromo-2-naphthoic acid (1 g, 3.98 mmol, Combi-Blocks, 98%), tetrabutylammonium hydroxide (19 mL, 40% in H_2O, Sigma-Aldrich), Cu_2O (0.028 g, 0.195 mmol, Alfa Aesar, 97%), 4,7-dihydroxy-1,10-phenanthroline (0.085 g, 0.401 mmol, Alfa Aesar), and deionized water (10 mL). The reactor was degassed with Argon for 5 min prior to pressurizing to 15 psi. The reaction temperature was gradually increased to 100°C and the starting materials allowed to react for 24 h. Afterward, the reaction was cooled to room temperature prior to venting to the atmosphere. The solution was then acidified to pH 2-3 with 2N HCl and extracted with ethyl acetate. The combined organic fractions were dried over anhydrous sodium sulfate and concentrated under vacuum. The crude product was further purified by column chromatography on silica gel using 1:1 hexane:ethyl acetate to obtain compound **1** as an off-white solid (0.581 g) in 77% yield: ^{1}H NMR (400 MHz, DMSO-d6): δ = 13.02 (s, 1H), 10.33 (s, 1H), 8.51 (d, J = 2 Hz, 1H), 8.21 (d, J = 9 Hz, 1H), 7.92 (dd, J = 2 Hz, 1H), 7.53 (d, J = 8 Hz, 1H), 7.40 (t, J = 8 Hz, 1H), 7.01 (d, J = 7.5 Hz, 1H). ^{13}C NMR (400 MHz, DMSO-d6): δ = 168.00, 153.59, 134.01, 130.60, 128.66, 127.82, 126.80, 124.25, 122.94, 120.18, 110.77.

Synthesis of 5-hydroxy-2-naphthoic acid methyl ester (**2**). Compound **1**, was dissolved in methanol (30 mL, Fischer, ACS grade) and cooled to < -20 °C in a dry ice/isopropanol (IPA) bath for 10 min. Thionyl chloride (3 eq, Aldrich, 97%) was then slowly added. The reaction was subsequently allowed to warm to room temperature and then was heated under reflux for 19h. Afterward, the solvent was removed by rotary evaporation. The product was dissolved in ethyl acetate (30 mL) and washed with brine (12 mL). The organic phase was collected and dried over anhydrous sodium sulfate and concentrated under vacuum. The crude product was further purified by column chromatography on silica gel using 2:1 hexane:ethyl acetate to obtain **2** as a pale yellow solid (0.510 g) in 74% yield, post lyophilization (stored under Argon until use): ^{1}H NMR (400 MHz, DMSO-d6): δ = 10.39 (s, 1H), 8.53 (d, J = 2 Hz, 1H), 8.23 (d, J = 9 Hz, 1H), 7.92 (dd, J = 2 Hz, 1H), 7.56 (d, J = 8 Hz, 1H), 7.41 (t, J = 8 Hz, 1H), 7.02 (dd, J = 1 Hz, 1H), 3.91 (s, 3H). ^{13}C NMR (400 MHz, DMSO-d6): δ = 166.90, 153.60, 133.94, 130.62, 128.04, 127.49, 126.89, 123.85, 123.20, 120.24, 111.02, 52.67. MS calculated for $C_{12}H_{10}O_3$: 202.06299, found: 202.06294.

Synthesis of 5-(hydroxymethyl)naphthalen-2-ol (**3**). To an Argon-charged round bottom flask equipped with an addition funnel was added **2** (510 mg, 2.52 mmol) and dry THF (25 mL, Acros). The solution was then cooled to -20 °C for 10 min in a dry ice/IPA bath. A slurry of lithium aluminum hydride (LAH, 191 mg, 5.03 mmol, Alfa Aesar, 97%) in dry THF (15 mL) was subsequently added dropwise over a period of 40 min while maintaining a temperature of < 0 °C. The mixture was then allowed to warm to RT and stirring continued overnight, under Argon. The reaction was quenched once reduction of the ester was observed by thin layer chromatography. Quenching of the reaction was accomplished by first cooling to 5 °C using an ice water bath. For 1 mg of LAH used in the reaction, 1 μL of deionized water, 1 μL of 15% KOH (aq), and 3 μL of deionized water were added, in that order, to quench the reaction. Afterward, the reaction mixture

was stirred for an additional 5 h. The crude product was then filtered, and the filtrate was concentrated under vacuum to give **3** as a sticky green solid (0.340 g, 77% yield): ^{1}H NMR (600 MHz, DMSO-d6): δ = 10.52 (s, broad, 1H), 8.08 (d, J = 9 Hz, 1H), 7.71 (d, J = 1.5 Hz, 1H), 7.37 (dd, J = 2 Hz, 1H), 7.27 (m, 2H), 6.83 (dd, J = 2 Hz, 1H), 5.33 (s, broad, 1H), 4.64 (s, 2H). ^{13}C NMR (600 MHz, DMSO-d6): δ = 154.04, 140.63, 134.85, 127.01, 124.42, 124.21, 124.10, 122.41, 118.30, 108.14, 63.48. MS calculated for $C_{11}H_{10}O_2$: 174.06808, found: 174.06811.

Synthesis of 5-diethylamino-2-nitrosophenol (**4**). The synthetic procedure reported by Ramm, et al. was followed in this process.[48] 3-Diethylaminophenol (6 g, 0.0363 mol, Aldrich, 97%) was dissolved in 13 mL of 12 N HCl and 8 mL water and was then cooled to 0 °C using an ice water bath. Next, a solution of $NaNO_2$ (2.5 g, 0.036 mol) in 18 mL water was added dropwise over a period of 1 h while keeping the reaction temperature between 0 and 5 °C. The resulting brown slurry was stirred for an additional 4 h and the crude product was collected by filtration, yielding the hydrochloride salt as a yellow precipitate. The hydrochloride salt was subsequently converted to the free amine by diluting in 300 mL 0.1 M aqueous $NaHCO_3$ and extracting with dichloromethane. The combined organic fractions were dried over anhydrous sodium sulfate and concentrated under vacuum to give **4** as a brick-red solid (3.405 g) in 48% yield: ^{1}H NMR (600 MHz, DMSO-d6): δ = 7.31 (d, J = 10 Hz, 1H), 6.91-6.89 (m, 1H), 5.75 (d, J = 2.5 Hz, 1H), 3.61 (m, 4H), 1.19 (t, J = 7 Hz, 6H). ^{13}C NMR (600 MHz, DMSO-d6): δ = 169.26, 157.58, 149.59, 134.88, 115.84, 95.51, 46.1, 14.5. IR (polyethylene/cm^{-1}: 1629, 1514. MS calculated for $C_{10}H_{14}O_2N_2$: 194.10553, found: 194.10558.

Synthesis of 9-diethylamino-2-hydroxymethyl-5H-benzo[a]phenoxazine-5-one (**5**). To a round bottom flask was added **3** (0.340 g, 1.95 mmol), **4** (0.417 g, 2.15 mmol) and dry dimethylformamide (DMF) (45 mL). The flask was equipped with a condenser and the mixture

was stirred at reflux for 4.5 h, under an Argon atmosphere. The solvent was removed with a stream of nitrogen and mild heating. The crude product was purified by column chromatography on silica gel, using a 1:2 hexane:ethyl acetate mobile phase to give **5** as a dark violet solid (0.160 g) in 23% yield: ^{1}H NMR (400 MHz, DMSO-d6): δ = 8.50 (s, 1H), 8.05 (d, J = 8.1 Hz, 1H), 7.60 (dd, J = 9.4, 2.4 Hz, 2H), 6.79 (dd, J = 9.1, 2.8 Hz, 1H), 6.61 (d, J = 2.7 Hz, 1H), 6.22 (s, 1H), 5.50 (t, J = 5.7 Hz, 1H), 4.71 (d, J = 5.6 Hz, 2H), 3.47 (q, J = 6.9 Hz, 4H), 1.15 (t, J = 7.0 Hz, 6H). ^{13}C NMR (400 MHz, DMSO-d6): δ = 182.33, 152.17, 151.15, 146.89, 146.76, 138.87, 131.94, 131.28, 128.32, 124.60, 125.41, 124.60, 121.04, 110.61, 104.91, 96.39, 63.10, 44.90, 12.91.

Synthesis of 9-diethylamino-5H-benzo[a]phenoxazine-5-one-2-carboxaldehyde (**6**), NR-CHO. Compound **5** (0.160 g, 0.458 mmol) was dissolved in dry dichloromethane (70 mL) in a round bottom flask. A magnetic stir bar was added and the solution was placed under an Argon atmosphere. Pyridinium chlorochromate (0.197 g, 0.916 mmol, Frontier, 98%) (PCC) was next added portion-wise over 1 h. The reaction mixture was stirred at room temperature overnight under Argon and quenched when thin layer chromatography showed complete oxidation of the alcohol. Excess PCC was quenched by slowly adding isopropanol (17 eq) and stirring for an additional 30 min. The solvent was removed by rotary evaporation and the resulting solid was dissolved in deionized water and extracted with ethyl acetate. The combined organic fractions were dried over anhydrous sodium sulfate and concentrated under vacuum. The crude product was purified by column chromatography on silica gel using 1:1 hexane:ethyl acetate as the mobile phase, giving **6** as a purple solid (0.041 g) in 29% yield: ^{1}H NMR (400 MHz, DMSO-d6): δ = 10.27 (s, 1H), 9.07 (dd, J = 2 Hz, 1H), 8.30 (d, J = 8 Hz, 1H), 8.15 (dd, J = 2 Hz, 1H), 7.71 (d, J = 9 Hz, 1H), 6.91 (dd, J = 3 Hz, 1H), 6.72 (d, J = 3 Hz, 1H), 6.39 (s, 1H), 3.54 (q, J = 7 Hz, 4H), 1.19 (t, J = 7 Hz, 3H). ^{13}C NMR (400 MHz, DMSO-d6): δ = 193.72, 181.51, 152.91, 151.79,

147.20, 138.15, 137.62, 134.74, 132.54, 131.70, 129.00, 126.54, 125.15, 111.35, 105.53, 96.49, 45.06, 29.48, 12.94. MS calculated for $C_{21}H_{18}O_3N_2$:346.37922, found: 346.37920.

RESULTS AND DISCUSSION

Cs(Zr,Mg)-SiO₂ catalyst structural characterization. The XRD patterns obtained from fumed silica, and the Cs(Zr,Mg)-SiO$_2$ and MgO catalysts are shown in Figure 1. Broad peaks centered near 2 θ = 21° were observed for the Cs(Zr,Mg)-SiO$_2$ catalyst and SiO$_2$, as is characteristic of silica-based materials;[10] the weaker broad peak of the former confirms that the silica structure has been modified by impregnation of the metal nitrates.[10, 14, 49] Hexagonal cesium nitrate was also observed in the Cs(Zr,Mg)-SiO$_2$ pattern, as evidenced by the sharp peaks centered at 2 θ = 19.9, 28.2, 34.8, 40.3, 45.4 and 50°, while no magnesium nitrate or zirconium nitrate species were detected. The latter suggests these components are well dispersed in the silica matrix.[14] Sharp peaks at 2 θ = 42.8 and 62.1°, and weaker peaks at 2 θ = 37, 74.7 and 78.7° were observed in the MgO XRD pattern and were attributed to the presence of its cubic phase.[50]

SEM and TEM images of the catalysts are shown in Figure 2. SEM images of the MgO catalyst and fumed silica (see Figures 2A,C) show agglomerated spherical particles of various sizes. When Mg, Zr, and Cs were loaded into the silica, the catalyst became more aggregated, as evidenced by the TEM image in Figure 2F. The surface area and porosity results for these materials are summarized in Table 1. The corresponding nitrogen sorption isotherms and pore size distributions are shown in Figures S1, S2.
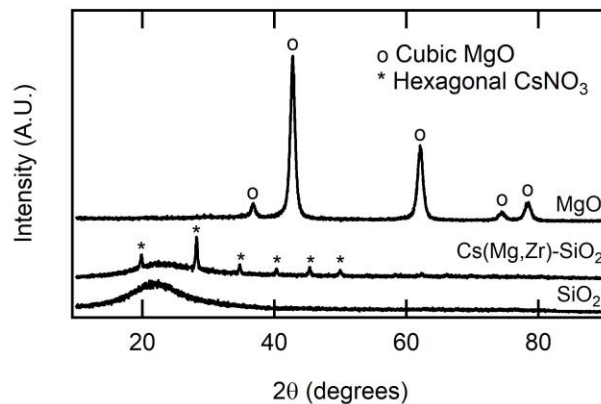
14

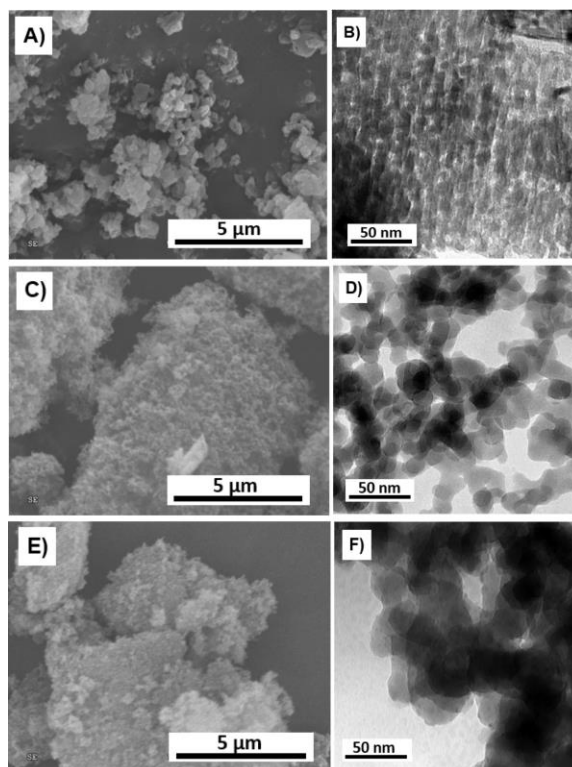**Figure 1.** X-Ray diffraction patterns from fumed silica along with $Cs(Zr,Mg)-SiO_2$ and MgO catalysts.

Figure 2. **A), B)** SEM and TEM images of commercial MgO catalyst particles. **C), D)** SEM and TEM images of SiO_2 particles. **E), F)** SEM and TEM images of $Cs(Zr,Mg)-SiO_2$ particles.

Catalyst chemical composition. EDS did not detect Mg or Zr on the $Cs(Zr,Mg)-SiO_2$ catalyst due to their low loadings of 0.025 wt.% and 0.033 wt.%, respectively, while a Cs content of 12.93 wt.% was measured, in agreement with the theoretical loading of 13 wt.%. ICP-OES

15

measurements detected all three metals.   In this case, the metal contents were determined to be

0.021 ± 0.001 wt.% for Mg, 0.0051 ± 0.0003 wt.% for Zr, and 11.4 ± 0.4 wt.% for Cs. The error

bars give the 95% confidence–intervals with n = 6 for Mg and Zr, and n = 9 in the case of Cs.

While the values obtained for Cs and Mg were close to their theoretical loadings, Zr was lower

than expected. This may be due to competition between the metals for active sites on the silica.[42]

The Mg content in commercial MgO was 53.18 wt.%.

XPS spectra (see Figure S2) show the Cs (3d) peaks for the $Cs(Zr,Mg)-SiO_2$ catalyst, but

Mg and Zr were not detected due to their low loadings. The Si (2p) peak is also observed for

fumed silica, the Mg (1s) peak for MgO, and the O (1s) peak for both catalysts and pure silica.

The binding energies for the active components in the catalysts were 724.6 eV - 742.7 eV for

suboxides of Cs in $Cs(Zr,Mg)-SiO_2$ and 1304.2 eV for Mg-O in MgO.

The density of base and acid sites on the catalysts were quantified by stepwise temperature-

programmed desorption (TPD) of CO_2 and NH_3. The results of these experiments are shown in

Figure S3. A higher desorption temperature indicates stronger basicity or acidity, while the area

under each desorption peak is proportional to the number of active sites.[51] The desorption profile

for SiO_2 showed no base or acid sites while that of the $Cs(Zr,Mg)-SiO_2$, and MgO were found to

have base and acid sites of various strengths.

The CO_2 desorption profile for $Cs(Zr,Mg)-SiO_2$ showed prominent peaks in the 75 - 175

°C range (weak base sites) and the 275 - 475 °C range (medium strength base sites), while for

MgO, a broad CO_2 desorption peak in the 75 - 475 °C range (weak-medium base sites) was

observed. The NH_3 desorption profile for $Cs(Zr,Mg)-SiO_2$ also showed one peak in the 75 - 175

°C range (weak acid sites) and a second, broader peak in the 250 - 475 °C range (medium strength

acid sites). The commercial MgO catalyst showed a prominent desorption peak in the 200 - 300

°C range, corresponding to medium strength acid sites.   The corresponding base and acid site densities determined from Figure S3 are shown in Table 1.

Elemental analyses and TPD data suggest that the metal nitrates in the Cs(Zr,Mg)-SiO$_2$ catalyst aid in enhancing the base and acid properties of the silica support.   The differences in strength and quantity of these sites within the catalyst led to differences in aldol product formation compared to the MgO catalyst, as will be discussed below.

Table 1. Chemical and structural properties of the catalysts

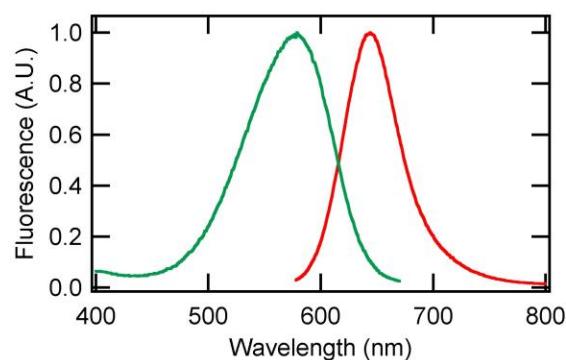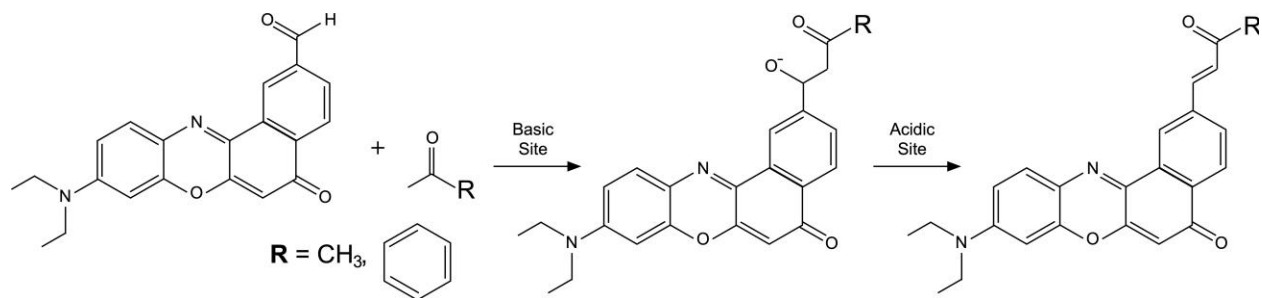| Catalysts	Basic site density (μmol CO$_2$/g)	Acid site density (μmol NH$_3$/g)	Metal content (%)	Total Surface Area$_{BET}$ (m^2/g)	Average Pore Diameter$_{BJH}$ (nm)	Total Pore Volume (cm^3/g) at p/p$_0$=0.99
MgO	820	791	Mg=53	119	8	0.32
SiO$_2$	0	0	-	194	12	0.50
Cs(Mg,Zr)-SiO$_2$	252	143	Cs=13, Mg<0.1 Zr<0.1	87	30	0.94

Figure 3. Fluorescence excitation (green) and emission (red) spectra of 1 μM NR-CHO in DMSO.

Scheme 2. Base-catalyzed aldol addition reactions, followed by acid-catalyzed dehydration reactions to form the aldol condensation products for reactions of NR-CHO (**6**) with ketones having **R** = methyl or phenyl.

Ensemble Fluorescence Studies of Aldol Reactions

Static spectra. Static fluorescence excitation and emission spectra of NR-CHO (1 μM) in DMSO are shown in Figure 3. The dye is most efficiently excited near 580 nm and emits most strongly near 645 nm. Static spectra of the newly synthesized NR-CHO were compared to that of commercial Nile Red under identical experimental conditions (Figure S4). The emission spectrum of NR-CHO is shifted ~ 18 nm to the red of commercial Nile Red.

Aldol reactions. Aldol reactions may be catalyzed by either base or acid.[12, 52-53] In this work, Cs(Zr,Mg)-SiO$_2$ having substantial base and acid sites was employed to catalyze reactions of NR-CHO (1 μM) in DMSO with acetone or acetophenone. The results obtained were compared to those of reactions catalyzed by commercially available MgO, while fumed silica served as a control. All reactions were conducted by stirring at room temperature.

Cs(Zr,Mg)-SiO$_2$ was chosen due to the extensive literature showing that aldol reactions are significantly enhanced when bifunctional catalysts incorporating both weak acid and base sites are employed.[15, 18, 45] It is believed that basic sites catalyze the aldol addition step, forming an alcohol, while acidic sites catalyze subsequent condensation to form the olefin product, as shown in Scheme 2. In Cs(Zr,Mg)-SiO$_2$, the cesium nitrate is believed to provide the base sites and some acid sites,

while SiOH groups on the silica likely provide additional acid functionality.   The magnesium and

zirconium aid in improving and maintaining the performance of the catalyst.[9, 42]

The progress of crossed aldol reactions was monitored in real time by recording a series of

fluorescence spectra at different time intervals. Figure 4 depicts the fluorescence spectra obtained.

These data show notable differences in how the spectra evolve in time when either Cs(Zr,Mg)-

SiO$_2$ or MgO was used as the catalyst.

When Cs(Zr,Mg)-SiO$_2$ was employed, a progressive blue shift in the emission spectrum of

the dye was observed as the reaction proceeded. Aldol reactions with acetone and acetophenone

showed gradual blue shifts of 16 nm and 8 nm, respectively, over the time the data were acquired

(see Figures 4A,D).   The gradual shift in fluorescence exhibited by the dye is concluded to result

from formation of two different products, the addition and condensation products, in the presence

of residual starting material, as confirmed by HPLC-MS, see below.   Note that the reaction

between NR-CHO and acetone catalyzed by Cs(Zr,Mg)-SiO$_2$ was faster than the others.   The

spectral shift to the blue appeared to be complete by 2 h in this case.   In contrast, the reaction

between NR-CHO and acetophenone took at least 8 h for the full spectral shift to develop.   The

differences in rates for aldol reactions using acetone and acetophenone is attributable to structural

differences in these ketones.   The reaction with acetone may be faster due to the presence of two

alpha carbons, providing two acidic hydrogens that may make the first step of the reaction more

kinetically favored.   Alternatively, the incorporation of the phenyl group on the acetophenone

precursor may make its reaction with NR-CHO more sterically hindered and slower.

When MgO served as the catalyst, NR-CHO reactions with both ketones led to the

appearance of a new peak that grew in time as the reaction progressed, giving an apparent

isoemissive point in the spectra (see Figures 4B, E).   In both cases, the original fluorescence peak

centered at ~ 642 nm subsided, while a new peak centered at ~ 615 nm grew over time.   The

appearance of two peaks and an isoemissive point are consistent with the presence of two different

species in the reaction mixture, likely NR-CHO and a new product, as confirmed by HPLC-MS,

see below.   As in the case of reactions catalyzed by $Cs(Zr,Mg)-SiO_2$, the reaction with acetone was

quicker than when acetophenone was employed.   Reaction mixtures with SiO_2 resulted in no

apparent fluorescence shift, as shown in Figures 4C, F, suggesting no reaction occurred.   This may

be attributed to insufficient base or acid sites in the SiO_2 to catalyze the reaction.[54]   Note that the

TPD analysis shown in Figure S3 revealed no detectable base or acid sites on the silica. The

stability of the NR-CHO dye in the presence of the active heterogeneous catalysts employed in

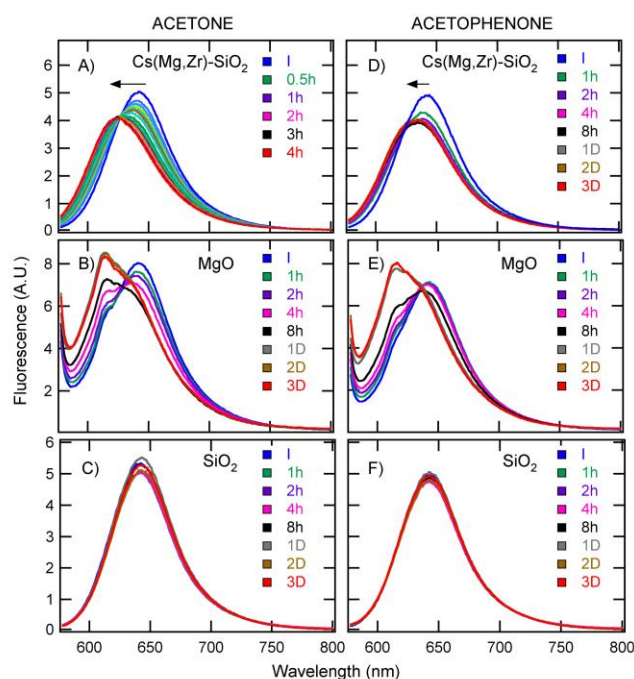this work was confirmed using solutions prepared without the ketone, see Figure S6.

Figure 4. A) - C) Fluorescence from NR-CHO as a function of time in the presence of the catalysts listed with acetone employed as the ketone. **D) - F)** Fluorescence from NR-CHO as a function of time in the presence of the catalysts listed with acetophenone employed as the ketone. Fluorescence was excited at 575 nm in each case.   DMSO was employed as the solvent.   All reactions were stirred at room temperature.

20

HPLC and LC-MS Studies of Aldol Product Formation

The differences in spectral behavior for the Aldol reactions catalyzed by Cs(Zr,Mg)-SiO$_2$ and MgO were attributed to the formation of different products. Analytical HPLC and HPLC-MS were employed to confirm that different products were formed in each case and to help identify these products. Representative chromatograms are provided in Figure 5 and the mass spectra used to assign each peak to the different products are given in Figure S5. As noted above, these reactions employed a higher concentration of NR-CHO (1mM) to facilitate product recovery and detection. The aldol reactions in this case were run for an arbitrary time of 3 days (see *kinetic measurements* below for further discussion).

Chromatograms obtained from aldol reactions employing Cs(Zr,Mg)-SiO$_2$ as the catalyst with acetone as the reactant were dominated by two peaks (see Figure 5A). HPLC-MS data allowed these two peaks to be assigned to the addition and condensation products (see Figure S5). The aldol addition product for this reaction gave a peak at 405 atomic mass units (amu, m/z) in the MS data, as expected, while the aldol condensation product gave a peak at 387 amu, as expected. Note that the mass resolution in this instrument is ± 1 amu. Separations performed using starting material alone revealed that one of the minor peaks was produced by residual NR-CHO. When acetophenone was employed as the reactant, the chromatograms obtained incorporated three peaks (see Figure 5C). HPLC-MS results (see Figure S5) allowed assignment of these peaks to the addition and condensation products, and residual NR-CHO. The chromatograph peak assigned to the aldol addition product gave a MS peak at 467 amu, while the condensation product produced a MS peak at 449 amu. In contrast, when MgO was employed as the catalyst, chromatograms obtained from both the acetone and acetophenone reaction mixtures were dominated by a single peak (see Figures 5B,D). HPLC-MS data obtained revealed these peaks were due to predominant

formation of the addition products and very little of the condensation products. The acetone addition product gave a MS peak at 405 amu, with the aldol condensation product yielding a MS peak at 387 amu. With acetophenone, the aldol addition product gave MS peaks at 467 amu and 449 amu for the addition and condensation products, respectively. These results provide strong support for the conclusions drawn from the spectroscopic data. The relatively large amount of un-reacted NR-CHO found in the reaction mixture with acetophenone when Cs(Zr,Mg)-SiO$_2$ was employed as the catalyst provides support for the conclusion that the kinetics are slowed as a result of ketone structure. The much smaller NR-CHO peak found when MgO was employed suggests it may be better than Cs(Zr,Mg)-SiO$_2$ at catalyzing the first step of the aldol reaction, while the Cs(Zr,Mg)-SiO$_2$ is better able to catalyze the subsequent condensation step. A more detailed discussion is given below.
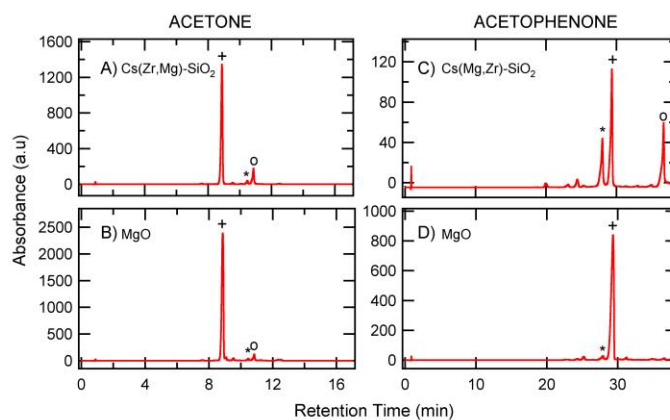

Figure 5. HPLC chromatograms (575 nm absorbance) of aldol products from 3-day reactions of NR-CHO (1mM) with acetone **(A, B)**, and acetophenone **(C, D)** in the presence of Cs(Zr,Mg)-SiO$_2$ or MgO at room temperature. The chromatograms show the un-reacted NR-CHO (*****), the aldol addition product (**+**), and the aldol condensation product (**o**). For **A, B,** the mobile phase gradient comprised H$_2$O and acetonitrile mixtures at 0.800 mL/min flow rate with the following compositions: 0-10 min: 95-40% H$_2$O; 10-15 min: 40-20% H$_2$O; 15-17 min: 20% H$_2$O. For **C, D** the mobile phase compositions were: 0-35 min: 95-45% H$_2$O; 35-36 min: 45-20% H$_2$O; 36-38 min: 20% H$_2$O. A Thermo Scientific Hypersil GOLD C18 column (100 X 3 mm^2, 3 μm particle size) was employed.

It is believed that the HPLC and HPLC-MS results for aldol reactions run at the higher NR-CHO concentration (1 mM) also reflect the products formed at the lower NR-CHO concentration (1 μM) employed in the spectroscopic studies. Therefore, the isoemissive points observed in aldol reactions catalyzed by MgO are attributed to the presence of primarily the un-reacted NR-CHO and the newly formed aldol addition product. Likewise, the gradual shifts in the spectra observed from aldol reactions employing the Cs(Zr,Mg)-SiO$_2$ catalyst (see Figures 4A, C) are attributed to the presence of time varying concentrations of un-reacted NR-CHO, the aldol addition product, and the aldol condensation product. Furthermore, spectra of the pure aldol products showed that both are blue shifted (alcohol by ~13-14 nm and olefin by ~2-4 nm), see Figure S7. The relatively small spectral blue shift of the olefin suggests that its fluorescence spectrum might be masked by unreacted NR-CHO in the reaction mixture. Since MgO primarily catalyzes aldol addition product formation, with its larger spectral shift, a clear peak at ~615 nm is distinguished in that mixture.

Aldol Reaction Kinetics

The kinetics of the crossed aldol reactions were followed using the fluorescence data shown in Figure 4. For this purpose, the fluorescence signals in two spectral bands spanning 642 ± 5 nm and 615 ± 5 nm were obtained and plotted as a function of time. This method was chosen over the usual procedure of fitting the data to multiple Gaussian functions because the latter did not provide robust, easily interpreted results on the disappearance of NR-CHO and the formation of products. Figure 6 shows the results of this analysis. These data show a time-dependent decrease in the 642 nm band that is concluded to reflect consumption of NR-CHO. Similarly, a time-dependent increase in the 615 nm band is observed that is interpreted to reflect appearance of the product(s). Note that control experiments employing fumed silica showed neither evidence for consumption of starting material nor appearance of product(s) (see Figure 6C,F).
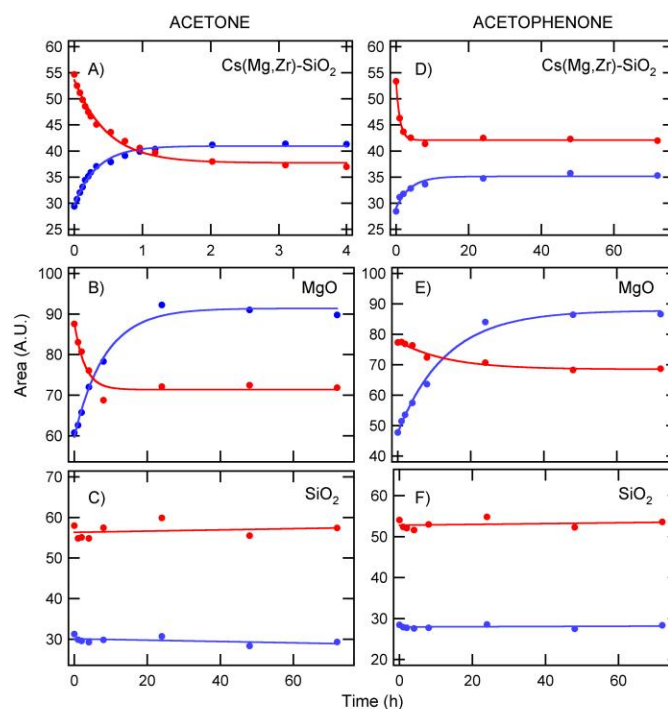
Figure 6. Fluorescence signals in bands spanning 642 ± 5 nm (red data points) and 615 ± 5 nm (blue data points) plotted as a function of time for crossed aldol reactions with acetone, **A)-C)**, and acetophenone, **D)-F)**. These data were obtained from Figure 4A-F. Data are given for reactions catalyzed by Cs(Zr,Mg)-SiO$_2$, **A), D)**, as well as MgO, **B), E)**, and the silica control, **C), F)**. The solid lines have been added to better depict the trends in the data. Note that the NR-CHO reaction with acetone catalyzed by Cs(Zr,Mg)-SiO$_2$ is significantly faster than the others.

The data in Figures 6A,B and 6D,E were employed to determine the rate of disappearance of NR-CHO and the rate of formation of aldol product(s). These rates were obtained by fitting the curves to single exponentials. Estimated rates of disappearance of NR-CHO in the reactions with acetone employing Cs(Zr,Mg)-SiO$_2$ and MgO catalysts were 2.1 ± 0.2 h^{-1} and 0.4 ± 0.1 h^{-1}, respectively, while the rates of aldol product formation were found to be 3.0 ± 0.2 h^{-1} and 0.12 ±0.02 h^{-1}, respectively. Similarly, the estimated rates of disappearance of NR-CHO in the reactions with acetophenone catalyzed by Cs(Zr,Mg)-SiO$_2$ and MgO were 1.0 ± 0.1 h^{-1} and 0.08 ±0.02 h^{-1}, respectively, while the rates of aldol product formation were 0.3 ± 0.1 h^{-1} and 0.08 ± 0.01 h^{-1},

respectively.   Since the ketones were present at much higher concentrations than the NR-CHO, these rates represent estimates of the pseudo-first-order rate constants for these reactions. It is noteworthy that HPLC-MS did not reveal significant self-condensation of acetone.   The above results show some complexities in interpreting the rates of aldol reactions obained using fluorescence spectroscopy.

Catalyst Dependent Product Formation

The results given above show that the aldol reactions catalyzed by $Cs(Zr,Mg)-SiO_2$ produced both addition products (alcohols) and condensation products (olefins). In contrast, those catalyzed by MgO produced primarily addition products and little condensation products.   The fluorescence results shown in Figure 4, demonstrate that the nature of the NR-CHO blue shift as the reaction progresses is diagnostic for catalyst activity. Catalysts that form a single product, the alcohol, produce spectra incorporating an isoemissive point. Catalysts that produce both addition and condensation products yield fluorescence spectra that gradually shift to the blue. The observed differences in the two catalysts are attributed to differences in surface area, as well as differences in acid and base site densities and strengths.   Since aldol condensation reactions involve two distinct reaction steps, these will be addressed separately below.

The likely mechanism for the addition reaction and the factors governing its rate will be discussed first.   Strong bases are commonly used as homogeneous catalysts in aldol reactions.[55] Therefore, strong base sites are likely to be important in initiating the reactions explored here on heterogeneous catalysts. Indeed, the results shown in Table 1 and in Figure S3 demonstrate that MgO has a much greater density of base sites (820 vs. 252 μmol CO_2/g in TPD experiments) and that the density of the stronger sites (CO_2 desorbed at 250 - 475 °C) is much greater than is the case for $Cs(Zr,Mg)-SiO_2$ (326.7 vs. 86.6 μmol CO_2/g in TPD experiments). The strong base sites

are best at abstracting acidic hydrogens on the alpha carbon(s) of the ketone. The nucleophilic enolate carbanion formed then attacks the electron-poor carbon of the aldehyde, forming the addition product. The literature on heterogeneous inorganic catalysts also suggests that the metal centers (M) can polarize the precursor carbonyls, increasing their reactivity.[17, 56] The greater density of strong base sites and the greater metal content of the MgO is thus consistent with the predominant formation of addition product.

The MgO catalyst was also found to have greater surface area than the $Cs(Zr,Mg)-SiO_2$ materials (see Table 1). The greater base strength, greater base site density, and greater surface area of the MgO suggests product formation should be faster in reactions where it is employed as the catalyst. However, the results shown in Figure 6 indicate these reactions are actually slower. The apparently slower kinetics of the addition reaction in the case of MgO may be due to the reversibility of this reaction, with the retro-Aldol reaction also being relatively fast.

A common theme in the modern literature on heterogeneous aldol reactions is that bifunctional catalysts are best suited to formation of the condensation products.[9, 16, 54, 56] This prior work also demonstrates that weaker acid sites better catalyze condensation than do strong acid sites.[15, 17] Strong acid sites are believed to react with basic sites in close proximity, forming catalytically inactive ion pairs.[8, 13] In contrast, weak acid sites are believed to remain active and can interact with the aldol addition products. The results shown in Figure S3 demonstrate that $Cs(Zr,Mg)-SiO_2$ incorporates more catalytically active weak acid sites (NH_3 desorbed at 75-175 °C) than does the MgO (NH_3 desorbed at 200-300ºC). The improved catalytic activity of $Cs(Zr,Mg)-SiO_2$ toward aldol condensation may be due to surface silanol groups intrinsic to the silica support as well as the presence of some water, which together facilitate proton exchange in the bifunctional catalyst.[15, 18] These weak acid sites act to protonate the products of the addition

reaction, catalyzing irreversible dehydration to form the condensation product (the olefin).[5, 56]   It

is this final step that is believed to lead to relatively fast and irreversible conversion of the addition

products in the $Cs(Zr,Mg)-SiO_2$ catalyzed reactions to condensation products.

While the model given above is most consistent with the present results, alternatives have

also been discussed in the literature.   For example, recent work claims that proton equilibration

with the anion is fast and that addition product formation is the rate-limiting step.[55]   While the

addition reaction may be rate limiting, the present results are consistent with the conclusion that

formation of the condensation product is critical to preventing the retro-aldol addition reaction

from occurring.   An alternative mechanism that has also been proposed is that the carbonyl on the

aldehyde can be activated by protonation by the weak acid (Si-OH) sites.   Nucleophilic attack of

the enolate formed by interaction of the ketone with the basic sites then forms the addition product

which then loses water to yield the condensation product.[17]   The authors state that by this acid-

base cooperative mechanism, a strong base may be replaceable by a weaker base as long as the

acid sites are strong enough to activate one of the reactants.[17]   This mechanism does not provide a

satisfactory explanation for the present results because the MgO catalyst, which contains stronger

acid sites, forms little of the condensation products.   The exact mechanism of aldol product

formation in the present studies has not yet been fully elucidated and will require further work.

Comparison of NR-CHO to a Commercially Available Dye

As a final demonstration of the utility of the NR-CHO dye in fluorescence studies of aldol

reactions, its performance was compared to that of commercially available 3-perylene-

carboxaldehyde.   These studies are described in Supplementary Information.   While the NR-CHO

dye in the presence of catalyst produced spectral shifts of 27 nm upon formation of the addition

product and smaller shifts of 16 nm and 8 nm when the condensation projects were also formed,

the commercial dye showed little or no change in its fluorescence emission spectrum, as shown in Figure S8. It should be noted that coumarin dyes incorporating either aldehyde or ketone moieties also show unique spectral shifts in response to aldol product formation.[57] However, these dyes are not well suited to single molecule studies, and the reactions reported were also performed at higher temperatures. In contrast, the aldol reactions presented here employed the NR chromophore widely used in single molecule studies,[36-37] and were run at room temperature, a condition more amenable to optical microscopic experiments. As a final caveat, it should be noted that spectral shifts similar to or larger than those exhibited by NR-CHO during addition product formation will be required for selective product detection in single molecule studies. The results obtained here suggest that it would be challenging to distinguish the condensation products from starting NR-CHO in single molecule studies. Further investigations using other ketones may afford greater spectral shifts.

CONCLUSIONS

In summary, we have synthesized a new form of the Nile Red dye, NR-CHO, incorporating a reactive aldehyde moiety to probe aldol reactions in real time through ensemble fluorescence measurements. Fluorescence from the dye exhibits a measurable blue shift when aldol addition and condensation products are formed. Catalysts that lead to formation of the addition product yield time-variant NR-CHO fluorescence spectra incorporating an isoemissive point, consistent with formation of a single product. When the condensation product is also formed, the fluorescence spectra instead exhibit a gradual shift to the blue, due to the presence of addition and condensation products, along with residual starting material. These observations allow for preliminary conclusions on catalyst activity to be drawn.

The NR-CHO fluorescence results in model reactions showed that product formation was dependent upon the type of catalyst employed.   These observations were confirmed by HPLC and HPLC-MS characterization of the reaction mixtures.   Reactions catalyzed by MgO yielded predominantly aldol addition products, while those catalyzed by $Cs(Zr,Mg)$-SiO_2 produced both addition (alcohol) and condensation (olefin) products. The $Cs(Zr,Mg)$-SiO_2 was shown to be more catalytically active towards olefin formation than MgO according to both fluorescence studies of the reaction kinetics and HPLC data.   Detailed analysis of the base and acid site densities and strengths demonstrated that the MgO catalyst contained the strong base sites necessary to catalyze the addition reaction, but that the acid sites also present were likely too strong to give the condensation product.   In contrast, the $Cs(Zr,Mg)$-SiO_2 catalyst was found to incorporate both the basic sites needed to initiate the addition reaction and weak acid sites of appropriate strength to drive dehydration and irreversible formation of the olefin.   Fumed silica was employed as a control and showed no activity due to the absence of active basic and acidic sites.   The newly synthesized NR-CHO was shown to be much more useful in following crossed aldol reactions than a commercially available 3-perylene carboxaldehyde, which showed little change in its fluorescence spectra during these reactions. The results presented here show that the NR-CHO dye is an effective fluorescent probe for *in situ* studies of aldol reactions of heterogeneous catalysts at the ensemble level.   The dye may also have promising future applications in studies of these same reactions at the single molecule level. Similar single molecule studies have been published describing investigations of other molecular transformations in organic chemistry.[58-60]

ACKNOWLEDGMENTS

REFERENCES

1. Weissermel, K.; Arpe, H.-J. Industrial Organic Chemistry. 3rd, Completely Revised Edition ed.; Wiley: 2008; p. 481.
2. Lippert, S.; Baumann, W.; Thomke, K. Secondary Reactions of the Base-Catalyzed Aldol Condensation of Acetone. *J. Mol. Catal.* **1991,** *69*, 199-214.
3. Zhang, G.; Hattori, H.; Tanabe, K. Aldol Addition of Acetone, Catalyzed by Solid Base Catalysts: Magnesium Oxide, Calcium Oxide, Strontium Oxide, Barium Oxide, Lanthanum (III) Oxide and Zirconium Oxide. *Appl. Catal.* **1988,** *36*, 189-197.
4. Izumi, Y.; Onaka, M. Liquid-Phase Organic Reactions Catalyzed by Inorganic Solid Acids and Bases. *J. Mol. Catal.* **1992,** *74*, 35-42.
5. Corma, A.; Iborra, S. Optimization of Alkaline Earth Metal Oxide and Hydroxide Catalysts for Base-Catalyzed Reactions. *Adv. Catal.* **2006,** *49*, 239-302.
6. Shylesh, S.; Thiel, W. R. Bifunctional Acid–Base Cooperativity in Heterogeneous Catalytic Reactions: Advances in Silica Supported Organic Functional Groups. *Chemcatchem* **2011,** *3*, 278-287.
7. Hruby, S. L.; Shanks, B. H. Acid–Base Cooperativity in Condensation Reactions with Functionalized Mesoporous Silica Catalysts. *J. Catal.* **2009,** *263*, 181-188.
8. Motokura, K.; Tada, M.; Iwasawa, Y. Acid–Base Bifunctional Catalytic Surfaces for Nucleophilic Addition Reactions. *Chem. Asian J.* **2008,** *3*, 1230-1236.
9. Li, B.; Yan, R.; Wang, L.; Diao, Y.; Li, Z; Zhang, S. Synthesis of Methyl Methacrylate by Aldol Condensation of Methyl Propionate with Formaldehyde Over Acid-Base Bifunctional Catalysts. *Catal. Lett.* **2013,** *143*, 829-838.
10. Wang, Y.; Lang, X.; Zhao, G.; Chen, H.; Fan, Y.; Yu, L.; Ma, X.; Zhu, Z. Preparation of Cs-La-Sb/SiO2 Catalyst and its Performance for the Synthesis of Methyl Acrylate by Aldol Condensation. *RSC Adv.* **2015,** *5*, 32826-32834.
11. Huh, S.; Chen, H.-T.; Wiench, J. W.; Pruski, M.; Lin, V. S.-Y. Cooperative Catalysis by General Acid and Base Bifunctionalized Mesoporous Silica Nanospheres. *Angew. Chem. Int. Ed.* **2005,** *44*, 1826-1830.
12. Dumitriu, E.; Hulea, V.; Fechete, I.; Auroux, A.; Lacaze, J. F.; Guimon, C. The Aldol Condensation of Lower Aldehydes Over MFI Zeolites with Different Acidic Properties. *Microporous Mesoporous Mater.* **2001,** *43*, 341-359.
13. Zeidan, R. K.; Hwang, S.-J.; Davis, M. E. Multifunctional Heterogeneous Catalysts: SBA-15-Containing Primary Amines and Sulfonic Acids. *Angew. Chem. Int. Ed.* **2006,** *45*, 6332-6335.
14. Li, B.; Yan, R.; Wang, L.; Diao, Y.; Li, Z.; Zhang, S. SBA-15 Supported Cesium Catalyst for Methyl Methacrylate Synthesis via Condensation of Methyl Propionate with Formaldehyde. *Ind. Eng. Chem. Res.* **2014,** *53*, 1386-1394.
15. Zeidan, R. K.; Davis, M. E. The Effect of Acid-Base Pairing on Catalysis: An Efficient Acid-Base Functionalized Catalyst for Aldol Condensation. *J. Catal.* **2007,** *247*, 379-382.
16. Brunelli, N. A.; Jones, C. W. Tuning Acid-Base Cooperativity to Create Next Generation Silica-Supported Organocatalysts. *J. Catal.* **2013,** *308*, 60-72.
17. Climent, M. J.; Corma, A.; Fornes, V.; Guil-Lopez, R.; Iborra, S. Aldol Condensations on Solid Catalysts: A Cooperative Effect between Weak Acid and Base Sites. *Adv. Synth. Catal.* **2002,** *344*, 1090-1096.

18. Yan, J.; Zhang, C.; Ning, C.; Tang, Y.; Zhang, Y.; Chen, L.; Gao, S.; Wang, Z.; Zhang, W. Vapor Phase Condensation of Methyl Acetate with Formaldehyde to Preparing Methyl Acrylate Over Cesium Supported SBA-15 Catalyst. *J. Ind. Eng. Chem.* **2015,** *25*, 344-351.

19. Hattori, H. Heterogeneous Basic Catalysis. *Chem. Rev*. **1995,** *95*, 537-558.

20. Luo, M.-F.; Zhong, Y.-J.; Yuan, X.-X.; Zheng, X.-M. TPR and TPD Studies of CuOCeO2 Catalysts for Low Temperature CO Oxidation. *Appl. Catal. A* **1997,** *162*, 121-131.

21. Ge, Q.; Huang, Y.; Qiu, F.; Li, S. Bifunctional Catalysts for Conversion of Synthesis Gas to Dimethyl Ether. *Appl. Catal. A* **1998,** *167*, 22-30.

22. Martins, G. V. A.; Berlier, G.; Bisio, C.; Coluccia, S.; Pastore, H. O.; Marchese, L. Quantification of Brønsted Acid Sites in Microporous Catalysts by a Combined FTIR and NH_3-TPD Study. *J. Phys. Chem. C* **2008,** *112*, 7193-7200.

23. Berteau, P.; Delmon, B. Modifed Alumninas: Relationship between Activity in 1-Butanol Dehydration and Acidity Measured by NH_3 TPD. *Catal. Today* **1989,** *5*, 121-137.

24. Copeland, G. T.; Miller, S. J. A Chemosensor-Based Approach to Catalyst Discovery in Solution and on Solid Support. *J. Am. Chem. Soc.* **1999,** *121*, 4306-4307.

25. Jarvo, E. R.; Evans, C. A.; Copeland, G. T.; Miller, S. J. Fluorescence-Based Screening of Asymmetric Acylation Catalysts through Parallel Enantiomer Analysis. Identification of a Catalyst for Tertiary Alcohol Resolution. *J. Org. Chem.* **2001,** *66*, 5522-5527.

26. Lewis, W. G.; Magallon, F. G.; Fokin, V. V.; Finn, M. G. Discovery and Characterization of Catalysts for Azide-Alkyne Cycloaddition by Fluorescence Quenching. *J. Am. Chem. Soc.* **2004,** *126*, 9152-9153.

27. Chen, P.; Zhou, X.; Andoy, N. M.; Han, K.-S.; Choudhary, E.; Zou, N.; Chen, G.; Shen, H. Spatiotemporal Catalytic Dynamics within Single Nanocatalysts Revealed by Single-Molecule Microscopy. *Chem. Soc. Rev*. **2014,** *43*, 1107-1117.

28. Chen, T.; Dong, B.; Chen, K.; Zhao, F.; Cheng, X.; Ma, C.; Lee, S.; Zhang, P.; Kang, S. H.; Ha, J. W.; Xu, W.; Fang, N. Optical Super-Resolution Imaging of Surface Reactions. *Chem. Rev*. **2017,** *117*, 7510-7537.

29. Ristanovic, Z.; Hofmann, J. P.; De Cremer, G.; Kubarev, A. V.; Rohnke, M.; Meirer, F.; Hofkens, J.; Roeffaers, M. B. J.; Weckhuysen, B. M. Quantitative 3D Fluorescence Imaging of Single Catalytic Turnovers Reveals Spatiotemporal Gradients in Reactivity of Zeolite H-ZSM-5 Crystals upon Steaming. *J. Am. Chem. Soc.* **2015,** *137*, 6559-6568.

30. Ristanovic, Z.; Kubarev, A. V.; Hofkens, J.; Roeffaers, M. B. J.; Weckhuysen, B. M. Single Molecule Nanospectroscopy Visualizes Proton-Transfer Processes within a Zeolite Crystal. *J. Am. Chem. Soc.* **2016,** *138*, 13586-13596.

31. Kumar, N.; Kalirai, S.; Wain, A. J.; Weckhuysen, B. M. Nanoscale Chemical Imaging of a Single Catalyst Particle with Tip-Enhanced Fluorescence Microscopy. *Chemcatchem* **2019,** *11*, 417-423.

32. Tachikawa, T.; Majima, T. Single-Molecule, Single-Particle Approaches for Exploring the Structure and Kinetics of Nanocatalysts. *Langmuir* **2012,** *28*, 8933-8943.

33. Esfandiari, N. M.; Blum, S. A. Homogeneous vs Heterogeneous Polymerization Catalysis Revealed by Single-Particle Fluorescence Microscopy. *J. Am. Chem. Soc.* **2011,** *133*, 18145-18147.

34. Tanaka, F.; Mase, N.; Barbas, C. F. Design and Use of Fluorogenic Aldehydes for Monitoring the Progress of Aldehyde Transformations. *J. Am. Chem. Soc.* **2004,** *126*, 3692-3693.

35. Guo, H.-M.; Tanaka, F. A Fluorogenic Aldehyde Bearing a 1,2,3-Triazole Moiety for Monitoring the Progress of Aldol Reactions. *J. Org. Chem.* **2009,** *74*, 2417-2424.

36. Dickson, R. M.; Norris, D. J.; Tzeng, Y.-L.; Moerner, W. E. Three-Dimensional Imaging of Single Molecules Solvated in Pores of Poly(acrylamide) Gels. *Science* **1996,** *274*, 966-969.

37. Hou, Y.; Bardo, A. M.; Martinez, C.; Higgins, D. A. Characterization of Molecular Scale Environments in Polymer Films by Single Molecule Spectroscopy. *J. Phys. Chem. B* **2000,** *104*, 212-219.

38. Fu, Y.; Ye, F.; Sanders, W. G.; Collinson, M. M.; Higgins, D. A. Single Molecule Spectroscopy Studies of Diffusion in Mesoporous Silica Thin Films. *J. Phys. Chem. B* **2006,** *110*, 9164-9170.

39. Kumarasinghe, R.; Higgins, E. D.; Ito, T.; Higgins, D. A. Spectroscopic and Polarization-Dependent Single-Molecule Tracking Reveal the One-Dimensional Diffusion Pathways in Surfactant-Templated Mesoporous Silica. *J. Phys. Chem. C* **2016,** *120*, 715-723.

40. Dutta, A. K.; Kamada, K.; Ohta, K. Langmuir-Blodgett Films of Nile Red: A Steady-State and Time-Resolved Fluorescence Study. *Chem. Phys. Lett.* **1996,** *258*, 369-375.

41. Dutta, A. K.; Kamada, K.; Ohta, K. Spectroscopic Studies of Nile Red in Organic Solvents and Polymers. *J. Photochem. Photobiol. A: Chem.* **1996,** *93*, 57-64.

42. Jackson, S. D.; Johnson, D. W.; Scott, J. D.; Kelly, G. J.; Williams, B. P. Catalysts for the Production of Unsaturated Acids or Esters. US 6,544,924 B1, 2003.

43. Barrett, E. P.; Joyner, L. G.; Halenda, P. P. The Determination of Pore Volume and Area Distributions in Porous Substances. 1. Computations from Nitrogen Isotherms. *J. Am. Chem. Soc.* **1951,** *73*, 373-380.

44. Brunauer, S.; Emmett, P. H.; Teller, E. Adsorption of Gases in Multimolecular Layers. *J. Am. Chem. Soc.* **1938,** *60*, 309-319.

45. Sakthivel, K.; Notz, W.; Bui, T.; Barbas, C. F. Amino Acid Catalyzed Direct Asymmetric Aldol Reactions: A Bioorganic Approach to Catalytic Asymmetric Carbon-Carbon Bond-Forming Reactions. *J. Am. Chem. Soc.* **2001,** *123*, 5260-5267.

46. Briggs, M. S. J.; Bruce, I.; Miller, J. N.; Moody, C. J.; Simmonds, A. C.; Swann, E. Synthesis of Functionalised Fluorescent Dyes and Their Coupling to Amines and Amino Acids. *J. Chem. Soc. Perkin Trans. 1* **1997**, 1051-1058.

47. Wang, Y.; Zhou, C.; Wang, R. Copper-Catalyzed Hydroxylation of Aryl Halides: Efficient Synthesis of Phenols, Alkyl Aryl Ethers and Benzofuran Derivatives in Neat Water. *Green Chem.* **2015,** *17*, 3910-3915.

48. Ramm, J. H.; Gartmann, N.; Brühwiler, D. Direct Synthesis and Fluorescent Imaging of Bifunctionalized Mesoporous Iodopropyl-Silica. *J. Coll. Interf. Sci.* **2010,** *345*, 200-205.

49. Wang, Y.; Yan, R.; Lv, Z.; Wang, H.; Wang, L.; Li, Z.; Zhang, S. Lanthanum and Cesium-Loaded SBA-15 Catalysts for MMA Synthesis by Aldol Condensation of Methyl Propionate and Formaldehyde. *Catal. Lett.* **2016,** *146*, 1808-1818.

50. Aramendía, M. A.; Benítez, J. A.; Borau, V.; Jiménez, C.; Marinas, J. M.; Ruiz, J. R.; Urbano, F. Study of MgO and Pt/MgO Systems by XRD, TPR, and ¹H MAS NMR. *Langmuir* **1999,** *15*, 1192-1197.

51. Faba, L.; Diaz, E.; Ordonez, S. Aqueous-Phase Furfural-Acetone Aldol Condensation Over Basic Mixed Oxides. *Appl. Catal. B: Environ.* **2012,** *113*, 201-211.

52. Denmark, S. E.; Bui, T. Lewis Base Catalyzed Enantioselective Aldol Addition of Acetaldehyde-Derived Silyl Enol Ether to Aldehydes. *J. Org. Chem.* **2005,** *70*, 10190-10193.

53. Corma, A.; García, H. Lewis Acids: From Conventional Homogeneous to Green Homogeneous and Heterogeneous Catalysis. *Chem. Rev.* **2003,** *103*, 4307-4366.

54. Tai, J.; Davis, R. J. Synthesis of Methacrylic Acid by Aldol Condensation of Propionic Acid with Formaldehyde over Acid-Base Bifunctional Catalysts. *Catal. Today* **2007,** *123*, 42-49.

55. Perrin, C. L.; Chang, K.-L. The Complete Mechanism of an Aldol Condensation. *J. Org. Chem.* **2016,** *81*, 5631-5635.

56. Lewis, J. D.; Van de Vyver, S.; Roman-Leshkov, Y. Acid-Base Pairs in Lewis Acidic Zeolites Promote Direct Aldol Reactions by Soft Enolization. *Angew. Chem. Int. Ed.* **2015,** *54*, 9835-9838.

57. Jagtap, A. R.; Stam, V. S.; Rajule, R. N.; Kanetkar, V. R. Synthesis of Highly Fluorescent Coumarinyl Chalcones Derived from 8-Acetyl-1,4,Diethyl-1,2,3,4-Tetrahydro-7H-Pyrano[2,3,-g]Quinoxalin-7-One and Their Spectral Characteristics. *Dyes Pigments* **2011,** *91*, 20-25.

58. Ng, J. D.; Upadhyay, S. P.; Marquard, A. N.; Lupo, K. M.; Hinton, D. A.; Padilla, N. A.; Bates, D. M.; Goldsmith, R. H. Single-Molecule Investigation of Initiation Dynamics of an Organometallic Catalyst. *J. Am. Chem. Soc.* **2016,** *138*, 3876-3883.

59. Rybina, A.; Lang, C.; Wirtz, M.; Grussmayer, K.; Kurz, A.; Maier, F.; Schmitt, A.; Trapp, O.; Jung, G.; Herten, D.-P. Distinguishing Alternative Reaction Pathways by Single-Molecule Fluorescence Spectroscopy. *Angew. Chem. Int. Ed.* **2013,** *52*, 6322-6325.

60. Easter, Q. T.; Blum, S. A. Organic and Organometallic Chemistry at the Single-Molecule, -Particle, and -Molecular-Catalyst-Turnover Level by Fluorescence Microscopy. *Acc. Chem. Res.* **2019,** *52*, 2244-2255.

TOC Art
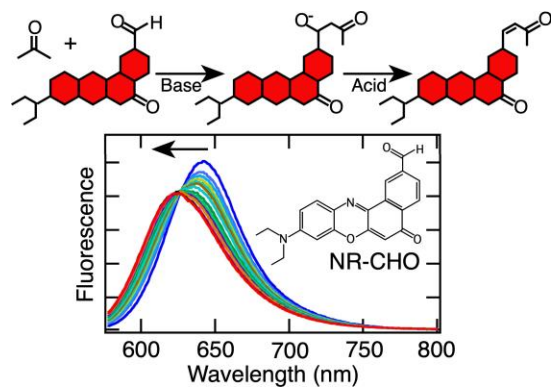
A highly fluorescent, aldol-reactive derivative of the dye Nile Red is synthesized and evaluated as an *in situ* probe of crossed aldol reactions.